Received: 12 May 2021 | Revised: 7 August 2021 | Accepted: 7 August 2021

DOI: 10.1111/jace.18070

Journal of the American Ceramic Society

RESEARCH ARTICLE

Up-conversion and temperature sensing properties of $Na_2GdMg_2(VO_4)_3$:Yb^{3+},Er^{3+} phosphors

LianJie Li[1] | **Ye Tong**[1] | **Jing Chen**[1] | **YiHang Chen**[1] | **Ghulam Abbas Ashraf**[1] | **LiPing Chen**[1] | **Tao Pang**[2] | **Hai Guo**[1]

[1]Department of Physics, Zhejiang Normal University, Jinhua, China

[2]College of science, Huzhou University, Huzhou, China

Correspondence
Hai Guo, Department of Physics, Zhejiang Normal University, Jinhua, 321004, China.
Email: ghh@zjnu.cn

Funding information
National Natural Science Foundation of China, Grant/Award Number: 11974315

Abstract

In this paper, $Na_2GdMg_2(VO_4)_3$:Yb^{3+},Er^{3+} phosphors were synthesized through high-temperature solid-state method. According to X-ray powder diffractogram, diffuse reflection spectra, scanning electron microscopy, up-conversion (UC) emission spectra, power-dependent UC spectra, fluorescent lifetime curves, and temperature-dependent emission spectra, the crystal structures, UC luminescent characteristics, and the performances of temperature sensing by using fluorescence intensity ratio technique were studied in detail. Heavy-doped phosphors with 59% (Yb^{3+} and Er^{3+}) doping content are achieved. In addition, excited by 980nm laser, three characteristic luminescence peaks of Er^{3+} at 525 nm ($^2H_{11/2} \rightarrow {}^4I_{15/2}$), 550 nm ($^4S_{3/2} \rightarrow {}^4I_{15/2}$) and 660 nm ($^4F_{9/2} \rightarrow {}^4I_{15/2}$) emerge in the UC spectra of Er^{3+} single-doped and Yb^{3+},Er^{3+} co-doped phosphors. UC spectra are dominated by green emission and greatly enhanced UC emission over 389 times is realized by introducing Yb^{3+}. In addition, the ratiometric techniques of thermally coupled energy levels of Er^{3+} (525/550 nm, $^2H_{11/2}/{}^4S_{3/2} \rightarrow {}^4I_{15/2}$) are used to achieve a wide range of temperature measurement. When the temperature is 303 K, relative sensitivity is as high as 0.976%K^{-1}. The minimal temperature resolution is 0.3 K@303 K. All experimental results show Yb^{3+},Er^{3+} co-doped $Na_2GdMg_2(VO_4)_3$ phosphors might act as optical temperature sensing materials.

KEYWORDS

fluorescence intensity ratio, $Na_2GdMg_2(VO_4)_3$:Yb^{3+},Er^{3+} phosphors, optical thermometers, up-conversion luminescence

1 | INTRODUCTION

Luminescent thermometers based on the temperature-dependent spectroscopic parameters are widely concerned because of their excellent accuracy, good sensitivity, and fast response.[1–6] Fluorescence intensity ratio (FIR) thermometry is deemed as a prospective optical temperature measurement approach in comparison with other optical temperature sensing techniques because it is independent of external factors, such as spectrum loss and excitation power fluctuations.[7–11] FIR technique has demonstrated superb anti-interference capabilities and improved sensitivity, especially for temperature measurements in electromagnetic and harsh environments, for example, the detection of building fire, the detection in micro/nano-meter scales, and biomedical imaging systems.[12–17] In general, FIR technique is realized by temperature-dependent fluorescence from thermal coupled energy levels (TCELs).[18–21]

Nowadays, Ho^{3+}, Er^{3+}, and Tm^{3+} ions are widely used as optical probes of temperature on account of their

TCELs.[19, 20, 22–25] Among these ions, Er^{3+} is considered as a promising emitter for detecting temperature because of its typical green up-conversion (UC) emission as well as the appropriate energy gap of TCELs (~700 cm^{-1}).[26–29] Whereas, 4f–4f transition of Er^{3+} is forbidden, which results in the small cross section of absorption at 980 nm and low UC intensity.[21, 30] Thus, to enhance the absorption near 980 nm, Yb^{3+} is usually selected as sensitizer.[31–34]

In recent years, vanadate-based phosphors have aroused extensive concerns.[19,35,36] Among vanadate phosphors, $Na_2GdMg_2(VO_4)_3$ is chosen as a superb substrate for rare-earth (RE) ions doping owing to the same valences and close ionic radii between Gd^{3+} and RE^{3+} ions.[37] For example, $Na_2GdMg_2(VO_4)_3$:Er^{3+} red phosphors with heavy doping concentration and excellent thermal stability were reported.[38] Consequently, the investigation of UC luminescence, the Yb^{3+}-Er^{3+} energy transfer (ET) and the temperature measurement performances of $Na_2GdMg_2(VO_4)_3$:Yb^{3+}, Er^{3+} samples are interesting and desired to be realized.

Herein, the $Na_2GdMg_2(VO_4)_3$:Yb^{3+}, Er^{3+} samples were elaborated to realize temperature sensing. According to X-ray powder diffractogram, diffuse reflection spectra, scanning electron microscopy, UC emission spectra, power-dependent UC spectra, fluorescent decay curves, and temperature-dependent emission spectra, the samples' crystal structure, UC luminescent characteristics, and temperature sensing performances by using FIR technology were studied in close detail.

2 | EXPERIMENTAL PROCEDURE

$Na_2GdMg_2(VO_4)_3$ (labeled as NGMVO), $Na_2Gd_{1-x}Mg_2(VO_4)_3$:xEr^{3+} (x = 0.01, 0.03, 0.05, 0.07, 0.09, and 0.11 in mol%) (labeled as NGMVO:xEr^{3+} (x = 0.01–0.11)) and $Na_2Gd_{0.91-y}Mg_2(VO_4)_3$:0.09$Er^{3+}$,$yYb^{3+}$ (y = 0, 0.2, 0.3, 0.4, 0.5, and 0.6) (labeled as NGMVO:0.09Er^{3+},yYb^{3+} (y = 0–0.6)) samples were fabricated through high-temperature solid-state technique in air atmosphere. The starting materials include Na_2CO_3, $MgCO_3$, NH_4VO_3 (A.R., all from Sinopharm Chemical Reagent Co., Ltd.), Gd_2O_3, Er_2O_3, Yb_2O_3 (99.99%, all from Yuelong New Materials Co., Ltd.). Firstl, all raw materials were ground to mix them evenly by adding a small amount of ethanol. Then the well-ground chemicals were put in the muffle furnace to pre-fire at 500°C for 5 h. After cooling down to the indoor temperature, the reagents were ground again for 5 min and then annealed in the muffle furnace at 750°C for 5 h. Eventually, all prepared products were reground to gain the final samples for further investigations.

X-ray powder diffractogram (XRD) of as-prepared products were obtained by using Rigaku MiniFlex/600 XRD equipment (Japan) with Cu Kα radiation, in which the angular range is from 10° to 80° in a step of 0.0167°. The microstructure of typical NGMVO:0.09Er^{3+},0.5Yb^{3+} phosphors was analyzed by Phenom ProX (Netherlands) scanning electron microscopy (SEM). The diffuse reflection spectra (DRS) of samples were taken by the Hitachi UH-4150 ultraviolet-visible-near infrared spectrophotometer (Japan). Fluorescence decay curves, room-temperature UC spectra were recorded by Edinburgh FS-5 spectrofluorometer (UK) assembled by a 980 nm laser with adjustable power. A TCB1402C temperature controller (China) was added for temperature-dependent UC spectra.

3 | RESULTS AND DISCUSSION

3.1 | Structural properties

Figure 1A shows the powder diffractograms of representative phosphors (NGMVO, NGMVO:0.09Er^{3+}, and NGMVO:0.5Yb^{3+},0.09Er^{3+}). XRD patterns of all samples

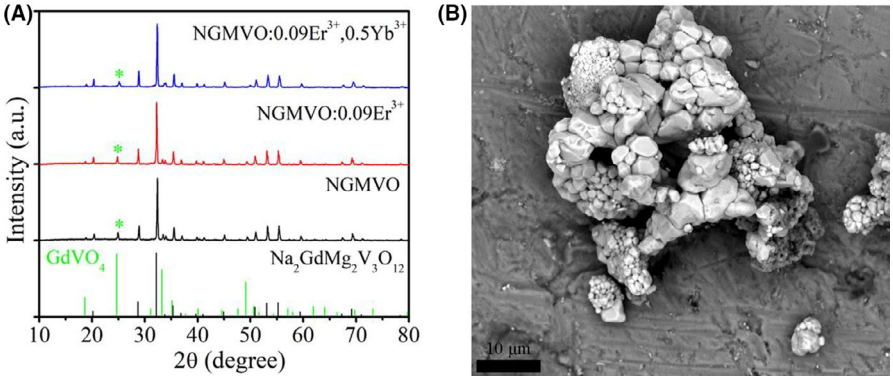

FIGURE 1 (A) Powder diffractograms of NGMVO, NGMVO:0.09Er^{3+}, NGMVO:0.5Yb^{3+},0.09Er^{3+} samples and the standard card of $GdVO_4$ (JSPDS No. 17–0260) and $Na_2GdMg_2V_3O_{12}$ (JCPDS No. 08–0510). (B) SEM photograph of NGMVO:0.5Yb^{3+},0.09Er^{3+} sample

display obvious sharp diffraction peaks. Except for some miscellaneous peaks in the range 24.5–25.5° (probably $GdVO_4$), they all match well with the standard XRD patterns of $Na_2GdMg_2V_3O_{12}$ with single cubic garnet structure.[38] And these impure diffraction peaks only occupy a relatively small proportion (smaller than 3.5%, has been proved in Figure S1B in supporting information file) in the entire crystal phase, which hardly affects their luminous properties. XRD patterns indicate that $Na_2GdMg_2V_3O_{12}$:Yb^{3+}, Er^{3+} phosphors were triumphantly synthesized. In addition, due to the similar radii and the same valence, Yb^{3+} and Er^{3+} will replace Gd^{3+}. It can be seen that after adding Yb^{3+} and Er^{3+}, the XRD patterns do not show a large deviation or other miscellaneous peaks, indicating that there is no change in the crystal phase.

Figure 1B presents the SEM image of representative NGMVO:0.5Yb^{3+},0.09Er^{3+} sample. The particles are anomalous in shape and uneven in size, and the size distribution is in the range 1–10 μm.

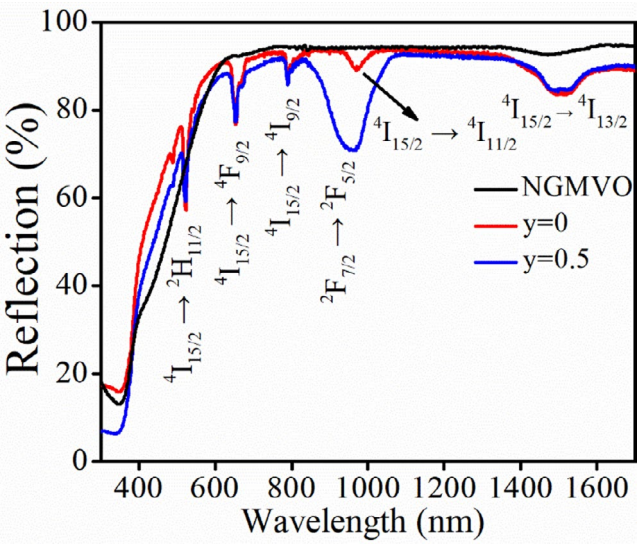

FIGURE 2 DRS spectra of NGMVO, NGMVO:0.09Er^{3+}, NGMVO:0.5Yb^{3+},0.09Er^{3+} samples

For the investigation on reflection of phosphors, NGMVO, NGMVO:0.09Er^{3+} and NGMVO:0.5Yb^{3+},0.09Er^{3+} were chosen to test DRS and corresponding results are displayed in Figure 2. Compared with undoped NGMVO, there are several absorption peaks attributed to the transitions of Er^{3+} ($^4I_{15/2} \rightarrow {}^2H_{11/2}$, $^4F_{9/2}$, $^4I_{9/2}$, $^4I_{11/2}$, and $^4I_{13/2}$) in NGMVO:0.09Er^{3+} as well as NGMVO:0.5Yb^{3+},0.09Er^{3+} phosphors, respectively.[20] Obviously, absorption peak near 980 nm of NGMVO:0.5Yb^{3+},0.09Er^{3+} is strengthened after introducing Yb^{3+}, which could be resulted from the transition of Yb^{3+} from $^2F_{7/2}$ to $^2F_{5/2}$.[19] The greatly enhanced absorption at 980 nm will contribute to greatly enhanced UC luminescence.

3.2 | UC luminescence properties

Figure 3A reveals the emission spectra of NGMVO:$x$$Er^{3+}$ (x = 0.1–0.11) materials with a laser radiation at 980 nm for exploring the UC properties. Three emission peaks at 525, 550, and 660 nm could be stemmed from transitions of Er^{3+} ($^2H_{11/2}$, $^4S_{3/2}$, and $^4F_{9/2} \rightarrow {}^4I_{15/2}$) in all Er^{3+} single-doped samples.[19] The whole emission intensity firstly increases and then decreases when $x > 0.09$ because of the concentration quenching. The optimal concentration of Er^{3+} is 9%.

To better assess the influence of the introduction of Yb^{3+} on luminescent properties of Er^{3+}, emission spectra of NGMVO:0.9Er^{3+},$y$$Yb^{3+}$ (y = 0–0.6) are shown in Figure 3B. The spectral shape and position of co-doped samples are similar to those of Er^{3+} single-doped samples. More importantly, it can be found that emission intensity of Er^{3+} is greatly increased with the introduction of Yb^{3+} and the maximal magnification is 389 times, which indicates the effective ET of Yb^{3+} → Er^{3+}. Besides, the optimal content of Yb^{3+} is 50%. Surprisingly, Yb^{3+} and Er^{3+} heavy-doped NGMVO phosphors were prepared and the concentration of doping reaches as high as 59%. What is more, from the Figure 3A,B, it can clearly see that green light dominates the emission area. The above-mentioned phenomena will

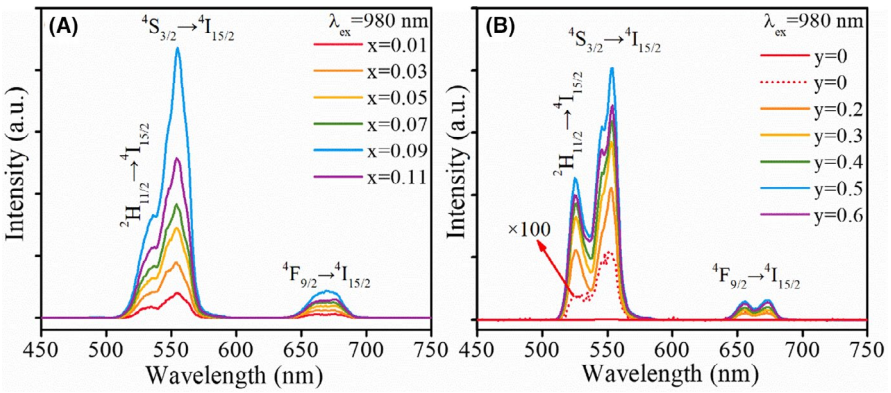

FIGURE 3 Emission spectra of (A) NGMVO:$x$$Er^{3+}$ (x = 0.01–0.11) and (B) NGMVO:0.09Er^{3+},$y$$Yb^{3+}$ (y = 0–0.6) phosphors

be beneficial to get good temperature sensing performances of NGMVO:Yb^{3+}, Er^{3+} phosphors.[24]

For the investigation of UC mechanism, power-dependent UC spectra were tested and the photon numbers (n) involved in UC process are estimated by using the next formula,[20, 23, 24]

$$I \propto P^n \quad (1)$$

where I denotes the emission intensity and P is the pump power. In order to make n clearer, the vertical axis is set as Lg(I) and the horizontal axis is set as Lg(P), therefore the calculated slope equals to n. The corresponding results are exhibited in Figure 4A. Slopes of 525, 550, and 660 nm emission peaks are 1.65, 1.59, and 1.42, respectively, which indicates that UC processes involved in the phosphors are two-photon processes.[19, 24, 36]

According to above results, energy levels and UC mechanism of Yb^{3+} and Er^{3+} in NGMVO:Yb^{3+}, Er^{3+} phosphors are depicted in Figure 4B. Upon a 980 nm laser radiation, Yb^{3+} at $^2F_{7/2}$ state is excited to $^2F_{5/2}$ state. After that, Yb^{3+} ion transfers its energy to Er^{3+} and non-radiatively relaxes to $^2F_{7/2}$ state from $^2F_{5/2}$ state. Er^{3+} at $^4I_{15/2}$ state is pumped to $^4I_{11/2}$ state resulted from the energy from Yb^{3+}. This process could be written as ET1: Er^{3+} ($^4I_{15/2}$) + Yb^{3+} ($^2F_{5/2}$) → Er^{3+} ($^4I_{11/2}$) + Yb^{3+} ($^2F_{7/2}$).[19, 32] Subsequently, Er^{3+} at $^4I_{11/2}$ state is promoted to $^4F_{7/2}$ state due to the energy from Yb^{3+}, which could be labeled as ET2: Er^{3+} ($^4I_{11/2}$) + Yb^{3+} ($^2F_{5/2}$) → Er^{3+} ($^4F_{7/2}$) + Yb^{3+} ($^2F_{7/2}$).[20, 23] After that, Er^{3+} at $^4F_{7/2}$ state non-radiatively relaxes to $^2H_{11/2}$, $^4S_{3/2}$, and $^4F_{9/2}$ states, respectively. Ultimately, Er^{3+} at these three states radiatively relaxes to $^4I_{15/2}$ state and gives 525, 550, and 660 nm emissions, respectively.

Figure 5 presents the temporal curves of 525 and 550 nm emissions in NGMVO:0.09Er^{3+},$y$$Yb^{3+}$ (y = 0, 0.2, 0.3, 0.4, 0.5, and 0.6), respectively. Specific average lifetime (τ) can be computed by the formula,[12, 22, 38]

$$\tau = \int tI(t)\mathrm{d}t / \int I(t)\mathrm{d}t, \quad (2)$$

here $I(t)$ are the emission intensities of 525 and 550 nm at time t. Complex UC luminescent process in NGMVO:Er^{3+}, Yb^{3+} phosphors might be the reason for multi-exponential decay curves.[19, 22] It can be observed that the lifetimes of the two levels of Er^{3+} ($^2H_{11/2}$/$^4S_{3/2}$) increase firstly and then decrease when $y > 0.5$. The variation tendency of lifetime with Yb^{3+} content is[39] consistent with that of emission intensity with Yb^{3+} content shown in Figure 3B.

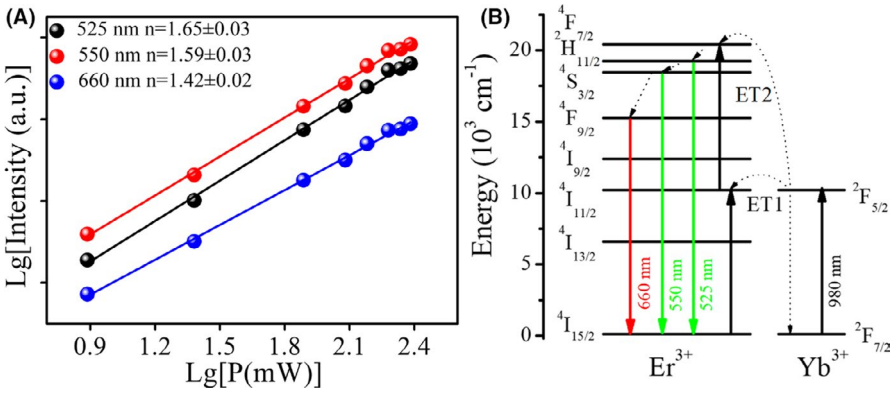

FIGURE 4 (A) The dependence of Lg(I) on Lg(P) of NGMVO:0.5Yb^{3+},0.09Er^{3+} phosphors. (B) Energy levels of Yb^{3+}, Er^{3+} and ET processes in NGMVO:Yb^{3+}, Er^{3+} phosphors

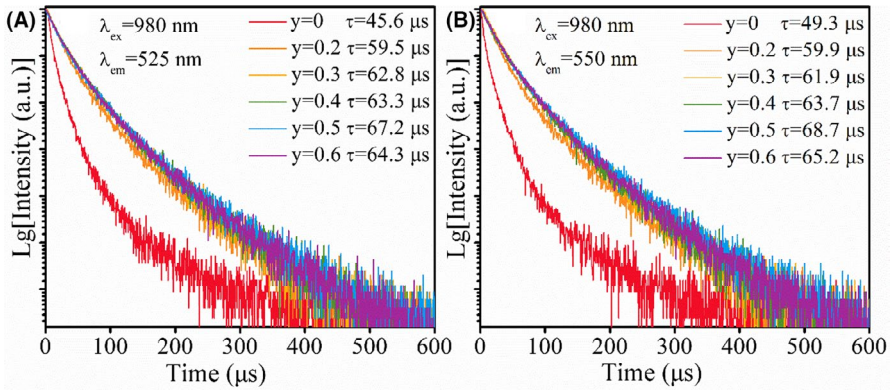

FIGURE 5 Fluorescent decay profiles of NGMVO:$y$$Yb^{3+}$,0.09$Er^{3+}$ at (A) 525 and (B) 550 nm, excited by 980 nm

3.3 | Optical temperature sensing performance

In general, the stronger the luminescence is, the greater the signal-noise ratio can be realized.[19] So NGMVO:0.5Yb^{3+},0.09Er^{3+} phosphors with the strongest green light emission were chosen to measure temperature sensing performance. Figure 6A gives the temperature-dependent spectra of NGMVO:0.5Yb^{3+},0.09Er^{3+} (303–573 K). Emission peak (525 nm) resulted from $^2H_{11/2} \rightarrow {}^4I_{15/2}$ transition of Er^{3+} firstly increases and then decreases. In the meanwhile, emission peak (550 nm) resulted from $^4S_{3/2} \rightarrow {}^4I_{15/2}$ transition of Er^{3+} continuously decreases as temperature increases. Normalized variable temperature spectra are shown in Figure 6B for a better comparison of band intensity ratio. Obviously, the emission intensity at 525 nm augments with the increase in temperature. FIR ($^2H_{11/2} \rightarrow {}^4I_{15/2}$ vs $^4S_{3/2} \rightarrow {}^4I_{15/2}$) can be correlated with temperature applying the below Boltzmann distribution law,[18, 19, 23, 40]

$$\mathrm{FIR} = \frac{I_H}{I_S} = \frac{N_H \omega_H A_H}{N_S \omega_S A_S} = \frac{g_H \omega_H A_H}{g_S \omega_S A_S} e^{-\frac{\triangle E}{k_B T}} = B e^{-\frac{\triangle E}{k_B T}}, \quad (3)$$

where I is the emission intensity from the transition of $^2H_{11/2}/{}^4S_{3/2} \rightarrow {}^4I_{15/2}$, respectively. g, A, N, *and* ω represent the degeneracy, the spontaneous emission probability, the number of Er^{3+} at different states as well as the angular frequency, respectively; B is $g_H\omega_H A_H / g_S \omega_S A_S$; T, ΔE, and k_B are Kelvin temperature, energy gap between TCELs of Er^{3+} ($^2H_{11/2}/{}^4S_{3/2}$) and Boltzmann constant.

According to Equation (3), corresponding fitting results are shown in Figure 7A. The equation for FIR and temperature can be written as following expression,

$$\mathrm{FIR} = 12.62 e^{\frac{-896.35}{T}}. \quad (4)$$

The fitting degree (R^2) is 0.997 and the thermal activation energy is 618 cm^{-1}.

As temperature sensing materials, absolute sensitivity (S_A) and relative sensitivity (S_R) can be estimated as below,[18, 20, 24, 37]

$$S_A = \left| \frac{\mathrm{d(FIR)}}{\mathrm{d}T} \right| = \frac{\Delta E}{k_B T^2} \mathrm{FIR}. \quad (5)$$

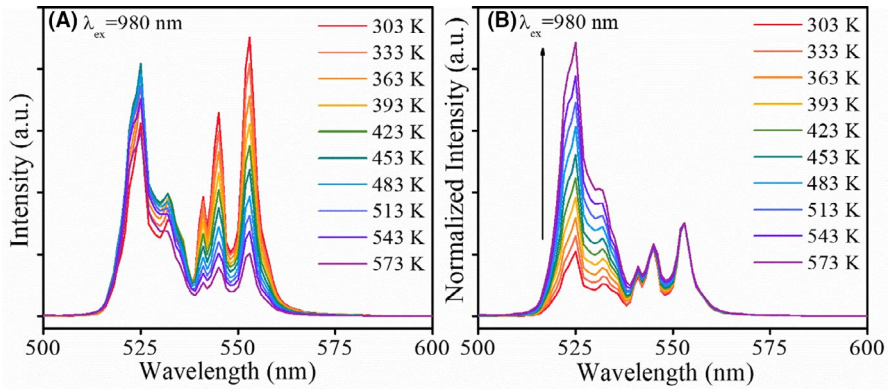

FIGURE 6 (A) Variable temperature spectra and (B) corresponding normalized temperature-dependent spectra of NGMVO:0.5Yb^{3+},0.09Er^{3+} sample (303–573 K)

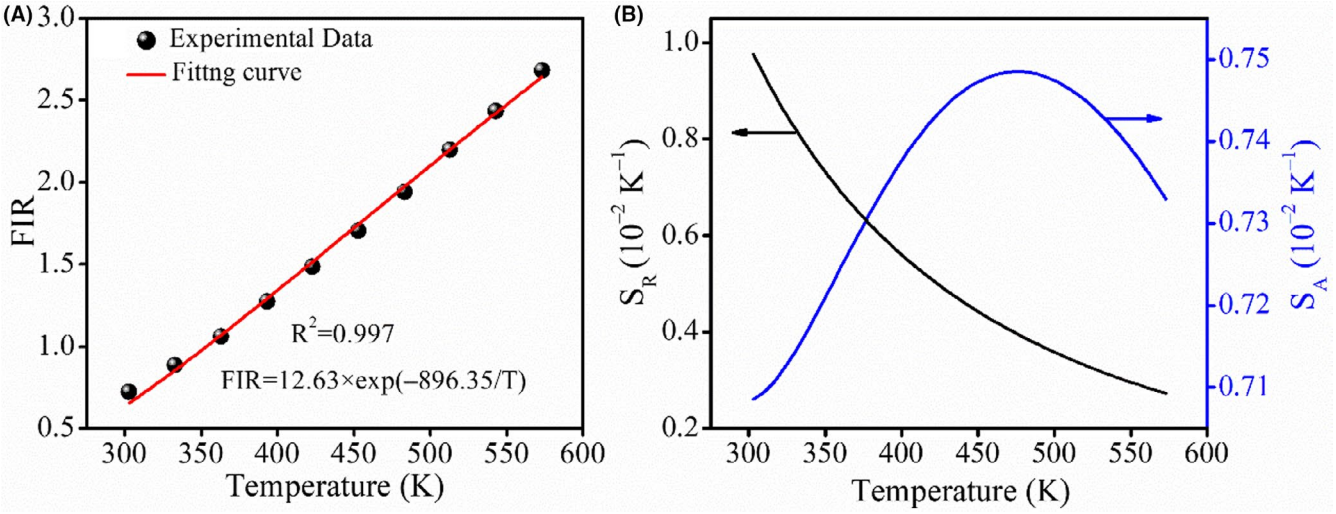

FIGURE 7 (A) FIR value, (B) absolute sensitivity and relative sensitivity of NGMVO:0.09Er^{3+},0.5Yb^{3+} sample (303–573 K)

TABLE 1 Optical parameters of various UC temperature sensing materials

Compounds	Temperature range (K)	$S_{R\text{-}MAX}$ ($\%K^{-1}$)	$S_{A\text{-}MAX}$ ($\%K^{-1}$)	References
$LuVO_4$:Nd, Yb, Er@SiO_2	295–338	1.4	1.22	[22]
$Ba_3Y_4O_9$:Yb, Er	83–563	/	0.248	[31]
Y_2O_3:Nd, Yb, Er@SiO_2@Cu_2S	293–420	1.2	0.5	[11]
Ca_2MgWO_6:Yb, Er	303–573	0.92	0.82	[20]
$LuVO_4$:Yb, Er@SiO_2	303–353	0.82	0.57	[33]
$NaYF_4$:Yb, Er	223–403	0.36	/	[39]
$Na_2GdMg_2(VO_4)_3$:Yb, Er	303–573	0.976	0.749	This work

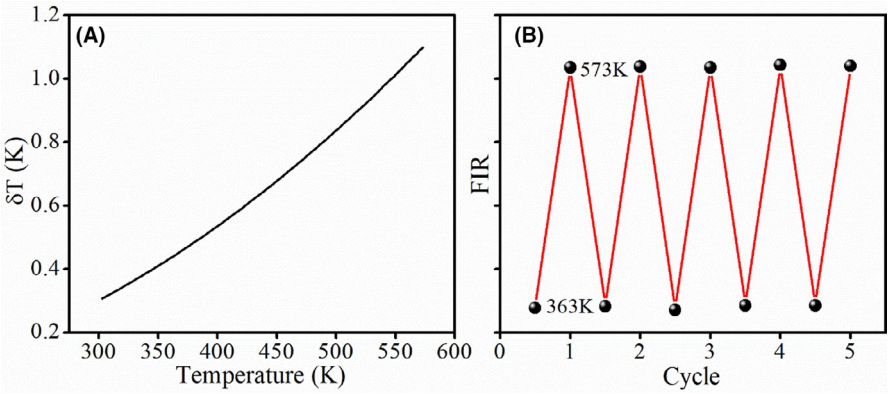

FIGURE 8 (A) Temperature resolution (303–573 K) and (B) repeatability (363 and 573 K) of NGMVO:0.5Yb^{3+},0.09Er^{3+} sample

$$S_R = \left| \frac{1}{\mathrm{FIR}} \frac{\mathrm{d(FIR)}}{\mathrm{d}T} \right| = \frac{\Delta E}{k_B T^2} \tag{6}$$

According to the above equations, calculated S_A and S_R values are described in Figure 7B. The maximal values of S_R and S_A are 0.976%K^{-1}@303 K and 0.749%K^{-1}@478 K, respectively. Table 1 gives the comparison of maximum sensitivities values of different optical temperature sensors. Compared with other reported FIR-based optical thermometric materials, a favorable $S_{R\text{-}MAX}$ value is obtained in this prepared $Na_2GdMg_2(VO_4)_3$:Yb^{3+}, Er^{3+} phosphors.

What is more, repeatability (R) and temperature resolution (δT) are important parameters in the field of temperature sensing, which can be deduced by following equations,[18,19]

$$\delta T = \frac{1}{S_R} \frac{\delta \Delta}{\Delta}, \tag{7}$$

$$R = 1 - \frac{\mathrm{Max}(\Delta_m - \Delta_i)}{\Delta_m}, \tag{8}$$

where $\delta\Delta/\Delta$, Δ_m, and Δ_i are accuracy parameters of the instrument, the average value of FIR and specific FIR values in five cycles (363 and 573 K), respectively. Specific results are given in Figure 8A,B. When temperature increases from 303 to 573 K, δT increases from 0.3 to 1.1 K. And R values (363 and 573 K) are bigger than 99%. The effect of Yb^{3+} doping on the temperature sensing properties was investigated also. As shown in Figure S2 and Table S1, FIR at different temperatures, S_A, S_R, and temperature resolution of different doping concentration of Yb^{3+} were calculated and compared. Results show that NGMVO:0.5Yb^{3+},0.09Er^{3+} phosphors with the strongest green light emission has the best temperature sensing performance. In summary, we can make a conclusion that NGMVO:Yb^{3+}, Er^{3+} phosphors using FIR technique show superior temperature sensing performances.

4 | CONCLUSION

A new type of green UC materials with $Na_2GdMg_2(VO_4)_3$:Yb^{3+}, Er^{3+} component was reported for temperature sensors. According to the above study, the following characteristics were obtained. Yb^{3+} and Er^{3+} heavy-doped NGMVO phosphors were achieved with a concentration of doping as high as 59%. Green light from $^2H_{11/2}/^4S_{3/2}$ TCELs of Er^{3+} dominates the emission spectra of $Na_2GdMg_2(VO_4)_3$:Yb^{3+}, Er^{3+}. UC emission of Er^{3+} is strengthened over 389 times by introducing Yb^{3+}. More importantly, the relative sensitivity maximum is 0.976%K^{-1} (303 K) by using FIR technology grounded on $^2H_{11/2}/^4S_{3/2}$ TCELs of Er^{3+}. And minimal temperature resolution is 0.3 K (303 K). All results above suggest Er^{3+}, Yb^{3+} co-doped $Na_2GdMg_2(VO_4)_3$ specimens might be applied as optical temperature sensors.

ACKNOWLEDGMENT

This work was supported by NSFC (No. 11974315).

ORCID

Tao Pang https://orcid.org/0000-0002-1747-972X
Hai Guo https://orcid.org/0000-0002-7867-0237

REFERENCES

1. Gao Y, Huang F, Lin H, Zhou J, Xu J, Wang Y. A novel optical thermometry strategy based on diverse thermal response from two intervalence charge transfer states. Adv Funct Mater. 2016;26(18):3139–45.
2. Dong B, Cao B, He Y, Liu Z, Li Z, Feng Z. Temperature sensing and in vivo imaging by molybdenum sensitized visible up-conversion luminescence of rare-earth oxides. Adv Mater. 2012;24(15):1987–93.
3. Brites C, Balabhadra S, Carlos L. Lanthanide-based thermometers: at the cutting-edge of luminescence thermometry. Adv Opt Mater. 2019;7(5):1801239.
4. Qiu X, Zhou Q, Zhu X, Wu Z, Feng W, Li F. Ratiometric upconversion nanothermometry with dual emission at the same wavelength decoded via a time-resolved technique. Nat Commun. 2020;11(1):1–9.
5. Zhuang B, Liu Y, Yuan S, Huang H, Chen J, Chen D. Glass stabilized ultra-stable dual-emitting Mn-doped cesium lead halide perovskite quantum dots for cryogenic temperature sensing. Nanoscale. 2019;11(32):15010–6.
6. Pan G, Zhang L, Wu H, Qu X, Wu H, Hao Z, et al. On the luminescence of Ti^{4+} and Eu^{3+} in monoclinic ZrO_2: high performance optical thermometry derived from energy transfer. J. Mater. Chem. C. 2020;8(13):4518–33.
7. Sekulic M, Dordevic V, Ristic Z, Medic M, Dramicanin M. Highly sensitive dual self-referencing temperature readout from the Mn^{4+}/Ho^{3+} binary luminescence thermometry probe. Adv Opt Mater. 2018;6(17):1800552.
8. Pan Y, Xie X, Huang Q, Gao C, Wang Y, Wang L, et al. Inherently Eu^{2+}/Eu^{3+} codoped Sc_2O_3 nanoparticles as high-performance nanothermometers. Adv Mater. 2018;30(14):1705256.
9. Chen X, Liu S, Huang K, Nie J, Kang R, Tian X, et al. Cr^{4+} activated NIR-NIR multi-mode luminescent nanothermometer for double biological windows. Chem Eng J. 2020;396:125201.
10. Wang C, Jin Y, Yuan L, Wu H, Ju G, Li Z, et al. A spatial/temporal dual-mode optical thermometry platform based on synergetic luminescence of Ti^{4+}-Eu^{3+} embedded flexible 3D micro-rod arrays: high-sensitive temperature sensing and multi-dimensional high-level secure anti-counterfeiting. Chem Eng J. 2019;374:992–1004.
11. Zhang Z, Suo H, Zhao X, Guo C. 808 nm laser triggered self-monitored photo-thermal therapeutic nano-system Y_2O_3:$Nd^{3+}/Yb^{3+}/Er^{3+}$@SiO_2@Cu_2S. Photonics Res. 2020;8(1):32–8.
12. Zheng Z, Zhang J, Liu X, Wei R, Hu F, Guo H. Luminescence and self-referenced optical temperature sensing performance in $Ca_2YZr_2Al_3O_{12}$:Bi^{3+}, Eu^{3+} phosphors. Ceram Int. 2020;46(5):6154–9.
13. Zhang H, Yang H, Li G, Liu S, Li H, Gong Y, et al. Enhancing thermometric performance via improving indicator signal in Bi^{3+}-doped $CaNb_2O_6$:Ln^{3+} (Ln = Eu/Sm/Dy/Tb) phosphors. Chem Eng J. 2020;396:125251.
14. Zhang X, Zhu Z, Guo Z, Sun Z, Chen Y. A ratiometric optical thermometer with high sensitivity and superior signal discriminability based on $Na_3Sc_2P_3O_{12}$:Eu^{2+}, Mn^{2+} thermochromic phosphor. Chem Eng J. 2019;356:413–22.
15. Li L, Tang X, Wu Z, Zheng Y, Jiang S, Tang X, et al. Simultaneously tuning emission color and realizing optical thermometry via efficient $Tb^{3+} \rightarrow Eu^{3+}$ energy transfer in whitlockite-type phosphate multifunctional phosphors. J Alloy Compd. 2019;780:266–75.
16. Gao Y, Cheng Y, Hu T, Ji Z, Lin H, Xu J, et al. Broadening the valid temperature range of optical thermometry through dual-mode design. J Mater Chem C. 2018;6(41):11178–83.
17. Li T, Guo C, Zhou S, Duan C, Yin M, Hintzen H. Highly sensitive optical thermometry of Yb^{3+}-Er^{3+} codoped $AgLa(MoO_4)_2$ green upconversion phosphor. J Am Ceram Soc. 2015;98(9):2812–6.
18. Dramićanin M. Trends in luminescence thermometry. J Appl Phys. 2020;128(4):040902.
19. Tong Y, Zhang W, Wei R, Chen L, Guo H. $Na_2YMg_2(VO4)_3$:Er^{3+}, Yb^{3+} phosphors: up-conversion and optical thermometry. Ceram Int. 2021;47(2):2600–6.
20. Jiang Y, Tong Y, Chen S, Zhang W, Hu F, Wei R, et al. A three-mode self-referenced optical thermometry based on up-conversion luminescence of Ca_2MgWO_6:Er^{3+}, Yb^{3+} phosphors. Chem Eng J. 2020;413:127470.
21. Lin M, Xie L, Wang Z, Richards B, Gao G, Zhong J. Facile synthesis of mono-disperse sub-20 nm $NaY(WO_4)_2$:Er^{3+}, Yb^{3+} up-conversion nanoparticles: a new choice for nanothermometry. J Mater Chem C. 2019;7(10):2971–7.
22. Chen D, Xu W, Yuan S, Li X, Zhong J. Ln^{3+}-sensitized Mn^{4+} near-infrared upconverting luminescence and dual-modal temperature sensing. J Mater Chem C. 2017;5(37):9619–28.
23. Cao J, Chen W, Xu D, Hu F, Chen L, Guo H. Wide-range thermometry based on green up-conversion of Yb^{3+}/Er^{3+} co-doped KLu_2F_7 transparent bulk oxyfluoride glass ceramics. J Lumin. 2018;194:219–24.
24. Chen S, Song W, Cao J, Hu F, Guo H. Highly sensitive optical thermometer based on FIR technique of transparent NaY_2F_7:Tm^{3+}/Yb^{3+} glass ceramic. J Alloy Compd. 2020;825:154011.
25. Zhang W, Tong Y, Hu F, Wei R, Chen L, Guo H. A novel single-phase $Na_{3.6}Y_{1.8}(PO_4)_3$:Bi^{3+}, Eu^{3+} phosphor for tunable and white light emission. Ceram Int. 2021;47(1):284–91.
26. Debasu M, Ananias D, Pastoriza-Santos I, Liz-Marzan L, Rocha J, Carlos L. All-in-one optical heater-thermometer nanoplatform operative from 300 to 2000 K based on Er^{3+} emission and blackbody radiation. Adv Mater. 2013;25(35):4868–74.
27. Cao B, Bao Y, Liu Y, Shang J, Zhang Z, He Y, et al. Wide-range and highly-sensitive optical thermometers based on the temperature-dependent energy transfer from Er to Nd in Er/Yb/Nd co-doped $NaYF_4$ upconversion nanocrystals. Chem Eng J. 2020;385:123906.
28. Li X, Wang X, Zhong H, Cheng L, Xu S, Sun J, et al. Effects of Er^{3+} concentration on down-/up-conversion luminescence and temperature sensing properties in $NaGdTiO_4$:Er^{3+}/Yb^{3+} phosphors. Ceram Int. 2016;42(13):14710–5.
29. Li X, Cao J, Wei Y, Yang Z, Guo H, Xie RJ. Optical thermometry based on up-conversion luminescence behavior of Er^{3+}-doped transparent Sr_2YbF_7 glass-ceramics. J Am Ceram Soc. 2015;98(12):3824–30.
30. Erdem M, Erguzel O, Ekmekci M, Orucu H, Cinkaya H, Genc S, et al. Bright white up-conversion emission from sol-gel derived $Yb^{3+}/Er^{3+}/Tm^{3+}$:Y_2SiO_5 nanocrystalline powders. Ceram Int. 2015;41(10):12805–10.

31. Wu H, Hao Z, Zhang L, Zhang X, Xiao Y, Pan G, et al. Er^{3+}/Yb^{3+} codoped phosphor $Ba_3Y_4O_9$ with intense red upconversion emission and optical temperature sensing behavior. J Mater Chem C. 2018;6(13):3459–67.
32. Guo H, Dong N, Yin M, Zhang W, Lou L, Xia S. Visible upconversion in rare earth ion-doped Gd_2O_3 nanocrystals. J Phys Chem B. 2004;108:19205–9.
33. Xiang G, Liu X, Zhang J, Liu Z, Liu W, Ma Y, et al. Dual-mode optical thermometry based on the fluorescence intensity ratio excited by a 915 nm wavelength in $LuVO_4:Yb^{3+}/Er^{3+}@SiO_2$ nanoparticles. Inorg Chem. 2019;58(12):8245–52.
34. Raju G, Pavitra E, Bharat L, Rao G, Jeon T, Huh Y, et al. Enhanced green up-conversion luminescence properties of Er^{3+}/Yb^{3+} co-doped strontium gadolinium silicate oxyapatite phosphor. Ceram Int. 2018;44(12):13852–7.
35. Song D, Guo C, Li T. Luminescence of the self-activated vanadate phosphors $Na_2LnMg_2V_3O_{12}$ (Ln = Y, Gd). Ceram Int. 2015;41(5):6518–24.
36. Savchuk O, Carvajal J, Cascales C, Aguilo M, Diaz F. Benefits of silica core-shell structures on the temperature sensing properties of Er, Yb:$GdVO_4$ up-conversion nanoparticles. ACS Appl Mater Interfaces. 2016;8(11):7266–73.
37. Cui S, Chen G. Enhanced up-conversion luminescence and optical thermometry characteristics of Er^{3+}/Yb^{3+} co-doped $Sr_{10}(PO_4)_6O$ transparent glass-ceramics. J Am Ceram Soc. 2020;103(12):6932–40.
38. Tong Y, Chen Y, Chen S, Wei R, Chen L, Guo H. Luminescent properties of $Na_2GdMg_2(VO_4)_3:Eu^{3+}$ red phosphors for NUV excited pc-WLEDs. Ceram Int. 2021;47:12320–6.
39. Dong B, Hua R, Cao B, Li Z, He Y, Zhang Z, et al. Size dependence of the unconverted luminescence of $NaYF_4$:Er,Yb microspheres for use in radiometric thermometry. Phys Chem Chem Phys. 2014;16:20009–12.
40. Xiang G, Liu X, Liu W, Wang B, Liu Z, Jiang S, et al. Multifunctional optical thermometry based on the stark sublevels of Er^{3+} in $CaO\text{-}Y_2O_3:Yb^{3+}/Er^{3+}$. J Am Ceram Soc. 2019;103(4):2540–7.

SUPPORTING INFORMATION

Additional Supporting Information may be found online in the Supporting Information section.

How to cite this article: Li L, Tong Y, Chen J, Chen Y, Abbas Ashraf G, Chen L, et al. Up-conversion and temperature sensing properties of $Na_2GdMg_2(VO_4)_3:Yb^{3+},Er^{3+}$ phosphors. J Am Ceram Soc. 2021;00:1–8. https://doi.org/10.1111/jace.18070